

DISCLAIMER

This document was prepared as an account of work sponsored by the United States Government. While this document is believed to contain correct information, neither the United States Government nor any agency thereof, nor The Regents of the University of California, nor any of their employees, makes any warranty, express or implied, or assumes any legal responsibility for the accuracy, completeness, or usefulness of any information, apparatus, product, or process disclosed, or represents that its use would not infringe privately owned rights. Reference herein to any specific commercial product, process, or service by its trade name, trademark, manufacturer, or otherwise, does not necessarily constitute or imply its endorsement, recommendation, or favoring by the United States Government or any agency thereof, or The Regents of the University of California. The views and opinions of authors expressed herein do not necessarily state or reflect those of the United States Government or any agency thereof, or The Regents of the University of California.

Ernest Orlando Lawrence Berkeley National Laboratory
is an equal opportunity employer.

**Detailed modeling and laser-induced fluorescence imaging of nitric oxide
in a NH₃-seeded non-premixed methane/air flame**

John B. Bell, Marcus S. Day, Joseph F. Grcar

Computing Sciences Directorate
Lawrence Berkeley National Laboratory
Berkeley, California, 94720, USA

Wolfgang G. Bessler, Christof Schulz

University of Heidelberg
Im Neuenheimer Feld 253
69120 Heidelberg, Germany

Peter Glarborg, Anker D. Jensen

Department of Chemical Engineering
Technical University of Denmark
DK-2800, Lyngby, Denmark

This work was supported under the SciDAC Program by the Director, Office of Science, Office of Advanced Scientific Computing Research, Mathematical, Information, and Computational Sciences Division of the U.S. Department of Energy, contract No. DE-AC03-76SF00098.

Detailed modeling and laser-induced fluorescence imaging of nitric oxide in a NH_3 -seeded non-premixed methane/air flame

Abstract

In this paper we study the formation of NO in laminar, nitrogen diluted methane diffusion flames that are seeded with ammonia in the fuel stream. We have performed numerical simulations with detailed chemistry as well as laser-induced fluorescence imaging measurements for a range of ammonia injection rates. For comparison with the experimental data, synthetic LIF images are calculated based on the numerical data accounting for temperature and fluorescence quenching effects. We demonstrate good agreement between measurements and computations. The LIF corrections inferred from the simulation are then used to calculate absolute NO mole fractions from the measured signal.

The NO formation in both doped and undoped flames occurs in the flame sheet. In the undoped flame, four different mechanisms including thermal and prompt NO appear to contribute to NO formation. As the NH_3 seeding level increases, fuel-NO becomes the dominant mechanism and N_2 shifts from being a net reactant to being a net product. Nitric oxide in the undoped flame as well as in the core region of the doped flames are underpredicted by the model; we attribute this mainly to inaccuracies in the NO recycling chemistry on the fuel-rich side of the flame sheet.

Introduction

Oxidation of fuel-bound nitrogen is the dominant source of nitrous oxides in combustion of solid fuels such as coal and biomass. Most of the fuel-nitrogen is released with the volatiles during devolatilization and subsequently oxidized in gas-phase diffusion flames. Despite the importance of fuel-NO, comparatively little work has been reported on conversion of reactive nitrogen species in non-premixed flames.

Laboratory studies of laminar diffusion flames doped with fuel-N have shown that speciation of gas-phase nitrogen compounds does not have a significant effect on NO yield [23]. The major parameters for fuel-N selectivity towards NO or N_2 appear to be the fuel-N dopant level and the flame configuration. At typical fuel-N/fuel ratios of about 1%, the conversion efficiency to NO is often below 30% [23, 29], in remarkable contrast to lean premixed flames where values of 80–100% have been reported for similar fuel-N seeding amounts [16, 34]. Despite the considerable progress over the last decade in modeling laminar non-premixed flames with detailed chemistry [2, 3, 12, 17, 25–28, 35], no study of fuel-nitrogen effects has been performed until recently.

Sullivan et al. [29] conducted a combined experimental and modeling investigation of NO_x formation in nitrogen-diluted laminar methane diffusion flames seeded with ammonia. The computations were performed with a two-dimensional model that included detailed chemical kinetics. The model showed good agreement with exhaust gas concentrations of NO over a wide range of NH_3 seeding. In particular, the declining efficiency of NH_3 to NO conversion with increased fuel-ammonia in nonpremixed flames [23] was observed both experimentally and in the simulations. Based on analysis of the calculations, the changes in NO formation and consumption mechanisms with increasing amounts of ammonia in the fuel were identified.

Even though the agreement between model and experiments in the work of Sullivan et al. was encouraging, flue concentration data alone is insufficient for model validation. For this purpose in-flame measurements are required, providing detailed characterization of the flame structure. In the present work we combine high-resolution numerical simulations and laser-induced fluorescence (LIF) imaging measurements for steady laminar diffusion flames with various levels of fuel-N. A similar approach was reported by Smooke et al. [25], but they do not consider fuel-N chemistry.

The present experimental set-up involves axisymmetric laminar coflowing non-premixed CH_4 /air flames doped with NH_3 , similar to those studied by Sullivan et al. The calculations were performed with a two-dimensional low Mach number model [8] combined with the reaction mechanism proposed by Glarborg et al. [13]. The objective of this work was partly to validate the model and partly to analyze further the NO formation mechanisms in non-premixed flames doped with fuel-N.

In the following sections we describe both the experimental setup and the computational methodology used in this study. We then provide a detailed comparison between the numerical results and the measured data. Finally, we discuss how added ammonia affects the nitrogen chemistry within the flames.

Experiment

Background

Laser-induced fluorescence has been frequently used as a non-intrusive technique for quantitative measurements of NO concentrations and temperatures in combustion processes. Quantitative NO-imaging has been performed in laminar [18] and turbulent [6, 20] atmospheric-pressure and high-pressure [5, 14] flames. LIF-based thermometry has been performed using the NO molecule as a temperature probe. Rotational [30] as well as vibrational [4] temperatures have been measured using one- [30], two- [4, 30] or multi-line [5, 32] techniques.

The dependence of NO-LIF intensity, I_{LIF} , for weak, non-perturbing laser excita-

tion is given by

$$I_{\text{LIF}} = c_{\text{cal}} I_{\text{laser}} N_{\text{NO}} \sum_i f_{B,i}(T) B_{i,k} g_{\lambda,i}(p, T, X) \sum_{k,j} \frac{A_{k,j}}{\sum_{\ell} A_{k,\ell} + Q_k(p, T, X)}. \quad (1)$$

I_{LIF} depends on the number density of the excitable molecules (number density N_{NO} times the Boltzmann fraction $f_{B,i}$), the Einstein coefficient $B_{i,k}$ for absorption $i \rightarrow k$, the spectral overlap fraction $g_{\lambda,i}(p, T, X)$ of the laser spectral profile and NO absorption spectrum and the fluorescence quantum yield $A/(\sum A + Q)$, where A and Q are decay rates due to spontaneous emission and electronic quenching, respectively. The summations account for overlapping transitions and rotational energy transfer in the excited state.

Q is calculated using temperature-dependent quenching cross-sections from Paul et al. [22]. The overlap fraction $g_{\lambda,i}$ is calculated using Doppler and pressure broadening as well as collisional shifting models [7, 9, 10, 33]. NO transition frequencies and rotational line strengths are calculated using relations from Paul [21], with vibrational transition probabilities from Laux and Kruger [15].

Equation 1 thus provides a quantitative relationship between I_{LIF} and the NO number density N_{NO} or mole fraction $X_{\text{NO}} = N_{\text{NO}} p/kT$. Its evaluation requires knowledge of temperature T and species mole fractions X .

Temperature is measured in a two-line approach using NO excitation from different vibrational ground states [4]. The large difference in ground state energies provides high temperature sensitivity at combustion temperatures (900–3000 K). The NO transitions used for thermometry and concentration measurements are the $A-X(0,0) R_{11} + Q_{21}(21.5)$ feature at 225.25 nm and the $A-X(0,2) O_{12}$ bandhead at 247.94 nm. The choice of these transitions was governed by the availability of a tunable KrF excimer laser that can be used directly or in combination with a hydrogen Raman cell to yield the required wavelengths in the (0,0) and (0,2) band, respectively [11].

Setup

The investigations were carried out in a modified Taran type burner [19] consisting of an inner (fuel, 1.0 cm diameter) and an outer (oxidizer, 3.25 cm diameter) tube. The reaction zone is enclosed by a fused silica tube (3.35 cm diameter) to stabilize the flame. Constant gas flows were provided by mass flow controllers (*Tylan, Bronkhorst*). For the fuel flow, methane (0.103 l/min) was diluted with nitrogen (0.151 l/min) and seeded with various amounts of NH_3 . Experimental and computational results are reported here for 0, 260, 420, 590, 790 and 1420 ppm of NH_3 seeding. Air (6.26 l/min) was used as oxidizer. For the temperature measurements, the fuel was seeded with 260 ppm NO (no NH_3) to yield high LIF-signal intensities in all regions of the flame.

The beam from a tunable, narrowband ($\Delta\nu = 0.6 \text{ cm}^{-1}$) KrF excimer laser (*Lambda Physik*, EMG 150) was used to pump a Raman shift cell (H_2 , 8 bar). The fundamental frequency (approx. 248 nm) and the first anti-Stokes line (approx. 225 nm) were separated by a Pellin-Broca prism and a slit aperture. Each laser beam was formed into a vertical light sheet ($30 \times 0.8 \text{ mm}^2$ cross-section) using a cylindrical lens and aligned with the center of the flame. The laser energy was detected by a fast photodiode. LIF-signals were focused (*Nikon*, $f = 105 \text{ mm}$, $f_{\#} = 4.5$) onto an intensified CCD camera (*LaVision*, StreakStar, 100 ns exposure time). Reflection bandpass filters in combination with a 248 nm short-pass filter were used to isolate the NO (0,1) fluorescence around 236 nm from LIF signal interference and elastically scattered light for both excitation wavelengths. The raw images were corrected for spatial and temporal laser energy fluctuations. The remaining background was corrected by taking data with the laser tuned off the NO resonance.

Calibration of both temperature and LIF signal was performed in a lean ($\phi = 0.92$) premixed ethylene/air flame. The temperature in this flame is known from CARS measurements [1]. The LIF signal was calibrated with NO seeding (100–1500 ppm) for the lean premixed flame [5, 31] assuming a loss of 10% of the added NO in the flame front due to reburn reactions.

Simulation methodology

The numerical simulations use a computational methodology [8] based on a low Mach number model. The axisymmetric model includes conservation equations for species mass and total enthalpy, and incorporates detailed chemical kinetics and thermodynamic relationships due to Glarborg, et al. [13], with transport properties from Sullivan et al. [29]. The numerical algorithm is based on a sequential predictor-corrector formulation, using a Godunov upwind method for the advection terms, and a semi-implicit (Crank-Nicholson) treatment of the diffusion. The chemical kinetics are integrated using implicit backward-difference methods. The low Mach number formulation introduces an elliptic constraint on the velocity field; the numerical approach applies a modified projection method to enforce this constraint on the solution.

The simulations use an adaptive numerical grid, where local grid resolution is concentrated in the flame zone. This adaptive methodology, incorporating the detailed nitrogen chemistry, has been shown to provide accurate predictions of NO_x formation in ammonia-enriched non-premixed flames [29]. Here, we discretize the entire quartz tube (radius: 1.675 cm, length: 30.15 cm). The grid-refinement criteria generates a five-level adaptive grid hierarchy, where each level is a factor of two finer than the next coarser one. The finest cells (in the flame zone) are approximately $65 \mu\text{m}$ on a side.

Comparison of Experiment and Simulation

Flame Height

The simulated and experimental flame showed a noticeable discrepancy in flame height. If h_f is the height above burner exit of the flame front in the center of the flame (corresponding to the rapid increase in NO concentration seen in Fig. 4 below), we find $h_{f,exp.} = 21.5$ mm and $h_{f,sim} = 30$ mm for the flame seeded with 1420 ppm NH_3 . We believe that this discrepancy arises from differences between the velocity profile at the burner exit and the profile used in the simulations. The simulations assume a fully developed laminar pipe flow but measurements to verify this assumption were not available. Nevertheless, the experimental and numerical flames are self-similar and the differences in the flame length do not appear to affect the chemistry. Therefore, for the remainder of the paper we scale the computational results vertically to match the experimental flame height. The resulting images shown here represent an area of $16 \times 30\text{mm}^2$.

Temperature Fields

Figure 1 compares experimental and computed temperature fields for the flames considered here. The temperature was measured with 260 ppm of NO seeded in the fuel for high LIF intensities throughout the flame. The vertical stripes at the sides of the flame are due to laser beam reflections on the quartz cylinder. The overall accuracy of the LIF temperature measurement is $\pm 5.5\%$ corresponding to $\approx 100\text{K}$ at the maximum flame temperature.

The agreement between measurement and computation is excellent. The principal differences are that the computations predict higher temperature in the lower portion of the flame and the measured temperature shows a slightly broader region of high temperature near the flame tip.

Comparison of Observed and Synthetic LIF Signals

Typically, experimental data is processed to obtain mole fractions of the quantity of interest for direct comparison to simulation results. As discussed above, conversion of the NO-LIF signal to quantitative NO mole fractions requires complex corrections for local temperature and species concentrations that are only known approximately. The quenching correction is particularly delicate for nonpremixed flames [24].

On the other hand, all of the data required to compute I_{LIF} are available from the simulation except the calibration constant c_{cal} which connects $I_{\text{LIF}}/I_{\text{laser}}$ to a standard LIF intensity emitted from a known NO concentration at the local T and X of the calibration flame. Rather than compare processed LIF data with simulations, we

compute synthetic NO-LIF images using the simulation results and compare those directly with the unprocessed LIF signals. The model then consists of both the simulation results (based on our understanding of fluid dynamics and chemical kinetics) and the fluorescence calculation (based on our understanding of NO molecular spectroscopy). The experimental data consists of the measured signal corrected for spatial variations in laser energy.

Figures 2 and 3 compare such “synthetic” with the calibrated, experimental LIF images for flames with different NH_3 seeding concentrations. The color code is scaled in arbitrary units proportional to calibrated NO-LIF intensities and is identical for the numerical and the experimental images. The data in Fig. 2 is from a lower ground state (A-X(0,0) excitation) resulting in a stronger signal from cold NO, while data in Fig. 3 corresponds to a higher ground state (A-X(0,2) excitation) that produces a stronger signal from hot NO.

As can be seen from the figures, the over-all agreement between the measured LIF and the synthetic LIF is excellent. For both cases, however, the simulations predict a weaker signal in the lower central part of the flame, which also shows slight differences in shape. Because of the different temperature sensitivity of the two data sets, and since temperatures are relatively low in this region (1000–1500K), this difference is much more pronounced in Fig. 2. With decreasing NH_3 seeding, the simulations increasingly underpredict the measured NO-LIF signals not only in the flame center, but also in the flame sheet.

The comparisons between the computed and measured temperatures and between the synthetic and measured NO-LIF show an overall good agreement.

NO Concentration

To investigate the quantitative agreement in more detail we derived NO concentrations from the experiment using quenching corrections obtained from the simulation data. This approach has been used before [25], though not for fuel-N seeded flames. Specifically, we use the NO A-X(0,0) data of Fig. 2, the experimental temperatures for Boltzmann and overlap fraction corrections, and the simulated major species concentrations to derive quenching corrections, according to equation (1). The resulting overall accuracy is $\pm 14\%$ for absolute NO concentrations and $\pm 10\%$ for relative values. Uncertainties of temperature, quenching rate, and the LIF experiment itself contribute approximately equal amounts to the total uncertainty.

Essentially the same concentrations were obtained by using NO A-X(0,2) data (not shown here). However, signal/noise decreased because of the higher temperature sensitivity and lower signal levels, leading to an uncertainty of up to $\pm 23\%$ in the colder central region of the flame.

Figure 4 displays the experimental and simulated NO concentration fields. Due to the corrections for temperature and fluorescence quenching, the spatial distribution

of NO differs from what might be anticipated by examining the LIF data in Fig. 2. In particular, the strong LIF signal in the central, cooler part of the flame observed in Fig. 2 is not actually indicative of an extremely high NO concentration.

NO concentration profiles are shown in Fig. 5. The profiles at 1 cm above the burner exit intersect the middle of the region of intense LIF signal in the lower part of the frames in Fig. 2. As already evident from the LIF images, the simulations underpredict NO concentrations in the cool center of the flame at this elevation. However, as can be seen in the right half of the figure, at higher elevations the agreement between experiment and simulation is very good for all but the lowest level of NH₃ seeding.

Discussion

Integrated Nitrogen Reaction Paths

To obtain a summary of the nitrogen chemistry we prepared integrated reaction path diagrams from the simulations. These show how nitrogen moves through the chemical species of the flames. Fig. 6 depicts the nitrogen chemistry for 0 and 1420 ppm of NH₃ seeding. The thickness of the arrows in these diagrams indicates the net number of nitrogen atoms (mol/s) transferred between species by chemical reactions, integrated over the simulation domain. Nitrogen *atoms* are used because as a conserved scalar they provide a consistent measure of the exchange of material among species due to reaction.

The diagrams reveal the extent to which the nitrogen chemistry is quickly dominated by fuel bound nitrogen. With no NH₃ seeding, all nitrogen chemistry stems from molecular nitrogen. Due to the large range of conditions occurring in the flame, no less than four mechanisms contribute to NO: thermal NO (initiating in paths $N_2 \rightarrow N, NO$), prompt NO (paths $N_2 \rightarrow N, HCN$), the N₂O (path $N_2 \rightarrow N_2O$), and the NNH mechanism (path $N_2 \rightarrow NNH$). With NH₃ added to the flame, fuel-NO becomes important. At 1420 ppm NH₃ seeding, the amine chemistry has reversed the net flow of nitrogen atoms out of molecular nitrogen, which is now a net product. In both doped and undoped flames there is considerable recycling of nitrogen through cyano species. The results are consistent with the observations of Sullivan et al. [29] who offer a detailed discussion of the nitrogen structure of these flames based on simulations.

Location of Peak NO Concentration

The fuel-nitrogen level affects not only the chemical mechanism for NO formation, but also the location of peak NO concentration. Thermal and prompt NO, which dominate at zero or low fuel-N levels, occur in the thin, parabola-shaped flame sheet.

As can be seen in the faint 0 ppm case of Fig. 4, NO concentrations just to the outside of the flame sheet increase with elevation leading to a peak in concentration downstream of the flame tip.

As the fuel-N seeding of the flame increases, however, the peak NO concentration spreads throughout the flame sheet (Fig. 4). Specifically, in the case of 1420 ppm NH₃ seeding, the simulation shows that a peak NO level of about 210 ppm occurs in a thin region that overlaps the parabola-shaped flame sheet. On the centerline, both peak NO and peak $T = 1810\text{K}$ occur at a height of $z = 2.1$ cm. The NO concentration drops off smoothly on the lean side of the flame as the NO mixes with other product gases.

NO in the Low-Temperature Flame Center

As the LIF images show, there is also some NO inside the low-temperature flame core. This can be attributed to diffusion and convection of NO and NO₂ from the flame sheet. The small amount of NO formed inside the core is largely due to reduction of NO₂, for instance by the reaction $\text{CO} + \text{NO}_2$. The major NO producing reaction in the flame sheet, $\text{N} + \text{OH} \rightarrow \text{NO} + \text{H}$, creates 0.26 mol/m²s of NO just inside the flame tip, at $z = 2.0$ cm, and reaches as high as 2.0 mol/m²s at the base of the flame sheet. This is four orders of magnitude more vigorous than any reactions that produce NO in the flame core.

The LIF images also show a very faint depletion zone for NO on the centerline. This is also indicated by the calculation. For example, for 1420 ppm NH₃ seeding, NO on the centerline has a local peak of 90 ppm at $z = 1.2$ cm, then dips to 77 ppm at $z = 1.8$ cm, before rising to 210 ppm at $z = 2.1$ cm at the flame tip. The slight drop is due to reactions such as $\text{CH}_3 + \text{NO} \rightarrow \text{H}_2\text{CN} + \text{OH}$. This occurs at the rate of about 10^{-5} mol/m²s over the range from $z = 1.5$ to 1.8 cm. For perspective on the strength of this reaction, it should be noted that the major NO consuming reaction is $\text{HCCO} + \text{NO} \rightarrow \text{HCN} + \text{CO}_2$; it is much more vigorous but it occurs just inside the flame sheet, peaking at 0.25 mol/m²s at $z = 2.0$ cm.

Due to the low temperatures and thereby low radical levels, the reactions consuming NO in the flame core are too slow to explain the differences between the measured and simulated NO concentrations in this region (Fig. 5). We attribute the discrepancy to overpredicting NO consumption on the fuel-rich side of the flame sheet and speculate that some refinement of the NO recycle chemistry, in particular related to the $\text{HCCO} + \text{NO}$ reaction, may improve the agreement between the measured and simulated NO concentrations in the low-temperature flame core, as well as the general agreement for the flames with low NH₃ seedings.

Concluding Remarks

The good agreement obtained between the experimental data and the simulations supports the present modeling approach and confirms that it is possible to describe the conversion of fuel nitrogen in laminar nonpremixed flames. Through analysis of the modeling results we can obtain a good understanding of details of the flame structure and the impact of physical and chemical parameters on the conversion selectivity of fuel nitrogen to NO and N₂. The ability to predict reliably the conversion of fuel-N as a function of process parameters in laminar nonpremixed flames is of significant interest, since there are important similarities to practical flames. This work represents a step forward towards the goal of understanding and modeling fuel-N conversion in practical combustors.

References

- [1] A. Arnold, B. Lange, T. Bouché, T. Heitzmann, G. Schiff, W. Ketterle, P. Monkhouse, and J. Wolfrum. Absolute temperature fields in flames by 2D-LIF of OH using excimer lasers and CARS spectroscopy. *Ber. Bunsenges. Phys. Chem.*, 96:1388–1392, 1992.
- [2] B. A. V. Bennett, C. S. McENally, L. D. Pfefferle, and M. D. Smooke. Computational and experimental study of axisymmetric coflow partially premixed methane/air flames. *Combust. Flame*, 123:522–546, 2000.
- [3] B. A. V. Bennett, C. S. McENally, L. D. Pfefferle, M. D. Smooke, and M. B. Colket. Computational and experimental study of axisymmetric coflow partially premixed ethylene/air flames. *Combust. Flame*, 127:2004–2022, 2001.
- [4] W. G. Bessler, F. Hildenbrand, and C. Schulz. Two-line laser-induced fluorescence imaging of vibrational temperatures in a NO-seeded flame. *Appl. Opt.*, 40:748–756, 2001.
- [5] W. G. Bessler, C. Schulz, T. Lee, D.-I. Shin, M. Hofmann, J. B. Jeffries, J. Wolfrum, and R. K. Hanson. Quantitative NO-LIF imaging in high-pressure flames. *Proc. Comb. Inst.*, 29, 2002. Submitted.
- [6] S. Böckle, J. Kazenwadel, T. Kunzelmann, and C. Schulz. Laser-diagnostic multi-species imaging in strongly swirling natural gas flames. *Appl. Phys. B*, 71:741–746, 2000.
- [7] A. Y. Chang, M. D. DiRosa, and R. K. Hanson. Temperature dependence of collision broadening and shift in the NO A \leftarrow X (0,0) band in the presence of argon and nitrogen. *J. Quant. Spectrosc. Radiat. Transfer*, 47:375–390, 1992.
- [8] M. S. Day and J. B. Bell. Numerical simulation of laminar reacting flows with complex chemistry. *Combust. Theory Modelling*, 4:535–556, 2000.
- [9] M. D. DiRosa and R. K. Hanson. Collision-broadening and -shift of NO $\gamma(0, 0)$ absorption lines by H₂O, O₂, and NO at 295K. *J. Mol. Spectrosc.*, 164:97–117, 1994.
- [10] M. D. DiRosa and R. K. Hanson. Collision broadening and shift of NO $\gamma(0, 0)$ absorption lines by O₂ and H₂O at high temperature. *J. Quant. Spectrosc. Radiat. Transfer*, 52:515–529, 1994.
- [11] T. Dreier, A. Dreizler, and J. Wolfrum. The application of a Raman-shifted tunable KrF excimer laser for laser-induced fluorescence combustion diagnostics. *Appl. Phys. B*, 55:381–387, 1992.

- [12] A. Ern, C. C. Douglas, and M. D. Smooke. Detailed chemistry modeling of laminar diffusion flames on parallel computers. *Int. J. Sup. App.*, 9:167–186, 1995.
- [13] P. Glarborg, M. U. Alzueta, K. Dam-Johansen, and J. A. Miller. Kinetic modelling of hydrocarbon/nitric oxide interactions in a flow reactor. *Combust. Flame*, 115:1–27, 1998.
- [14] F. Hildenbrand, C. Schulz, J. Wolfrum, F. Keller, and E. Wagner. Laser diagnostic analysis of NO formation in a direct injection diesel engine with pump-line-nozzle and common rail injection systems. *Proc. Comb. Inst.*, 28:1137–1144, 2000.
- [15] C. O. Laux and C. H. Kruger. Arrays of radiative transition probabilities for the N₂ first and second positive, NO beta and gamma, N₂⁺ first negative, and O₂ Schumann-Runge band systems. *J. Quant. Spectrosc. Radiat. Transfer*, 48:9–24, 1992.
- [16] R. J. Martin and N. J. Brown. Nitrous oxide formation and destruction in lean, premixed combustion. *Combust. Flame*, 80:238–255, 1990.
- [17] C. S. McEnally, L. D. Pfefferle, A. M. Schaffer, M. B. Long, R. K. Mohammed, M. D. Smooke, and M. B. Colket. Characterization of a coflowing methane/air non-premixed flame with computer modelling, Rayleigh-Raman imaging, and on-line mass spectrometry. *Proc. Comb. Inst.*, 28:2063–2070, 2000.
- [18] A. V. Mokhov, H. B. Levinsky, and C. E. van der Meij. Temperature dependence of laser-induced fluorescence of nitric oxide in laminar premixed atmospheric-pressure flames. *Appl. Opt.*, 36:3233–3243, 1997.
- [19] K. Müller-Dethlefs, M. Peleat, and J.-P. Taran. Temperature and hydrogen concentration measurements by CARS in an ethylene-air-bunsen flame. *Ber. Bunsenges. Phys. Chem.*, 85(9):803–807, September 1981.
- [20] M. Namazian, J. Kelly, and R. Schefer. Simultaneous NO and temperature imaging measurements in turbulent nonpremixed flames. *Proc. Comb. Inst.*, 25:1149–1157, 1994.
- [21] P. H. Paul. Calculation of transition frequencies and rotational line strengths in the γ -bands of nitric oxide. *J. Quant. Spectrosc. Radiat. Transfer*, 57:581–589, 1997.
- [22] P. H. Paul, J. A. Gray, J. L. Durant Jr., and J. W. Thoman Jr. A model for temperature-dependent collisional quenching of NO A² Σ^+ . *Appl. Phys. B*, 57:249–259, 1993.

- [23] A. F. Sarofim, G. C. Williams, M. Modell, and S. M. Slater. Conversion of fuel nitrogen to nitric oxide in premixed and diffusion flames. *AIChE Symp. Ser.*, 71(148):51–61, 1975.
- [24] V. Sick, F. Hildenbrand, and P. Lindstedt. Quantitative laser-based measurement and detailed chemical kinetic modeling of nitric oxide concentrations in methane-air counterflow diffusion flames. *Proc. Comb. Inst.*, 27:1401–1409, 1998.
- [25] M. D. Smooke, A. Ern, M. A. Tanoff, B. A. Valdati, R. K. Mohammed, D. F. Marran, and M. B. Long. Computational and experimental study of NO in an axisymmetric laminar diffusion flame. *Proc. Comb. Inst.*, 26:2161–2170, 1996.
- [26] M. D. Smooke, P. Lin, J. K. Lam, and M. B. Long. Computational and experimental study of a laminar axisymmetric methane-air diffusion flame. *Proc. Comb. Inst.*, 23:575–582, 1990.
- [27] M. D. Smooke, C. S. McEnally, L. D. Pfefferle, R. J. Hall, and M. B. Colket. Computational and experimental study of soot formation in a coflow, laminar diffusion flame. *Combust. Flame*, 117:117–139, 1999.
- [28] M. D. Smooke, R. E. Mitchell, and D. E. Keyes. Numerical solution of two-dimensional axisymmetric laminar diffusion flames. *Combust. Sci. Tech.*, 67:85, 1989.
- [29] N. Sullivan, A. Jensen, P. Glarborg, M. S. Day, J. F. Grcar, J. B. Bell, C. Pope, and R. J. Kee. Ammonia conversion and NO_x formation in laminar coflowing nonpremixed methane-air flames. *Combust. Flame*, 2001. Submitted.
- [30] M. Tamura, J. Luque, J. E. Harrington, P. A. Berg, G. P. Smith, J. B. Jeffries, and D. R. Crosley. Laser-induced fluorescence of seeded nitric oxide as a flame thermometer. *Appl. Phys. B*, 66:503–510, 1998.
- [31] D. D. Thomsen and N. M. Laurendeau. LIF measurements and modeling of nitric oxide concentration in atmospheric counterflow premixed flames. *Combust. Flame*, 124:350–369, 2001.
- [32] A. O. Vydrov, J. Heinze, M. Dillmann, U. E. Meier, and W. Stricker. Laser-induced fluorescence thermometry and concentration measurements on NO A-X (0,0) transitions in the exhaust gas of high pressure CH₄/air flames. *Appl. Phys. B*, 61:409–414, 1995.
- [33] A. O. Vydrov, J. Heinze, and U. E. Meier. Collisional broadening of spectral lines in the A-X (0-0) system of NO by N₂, Ar, and He at elevated pressures

measured by laser-induced fluorescence. *J. Quant. Spectrosc. Radiat. Transfer*, 53:277–287, 1995.

- [34] J. O. L. Wendt and C. V. Sternling. Effect of ammonia in gaseous fuels on NO_x emissions. *J. Air Poll. Control Ass.*, 24:1055–1058, 1974.
- [35] Y. Xu, M. D. Smooke, P. Lin, and M. B. Long. Primitive variable modeling of multidimensional laminar flames. *Combust. Sci. Tech.*, 90:289, 1993.

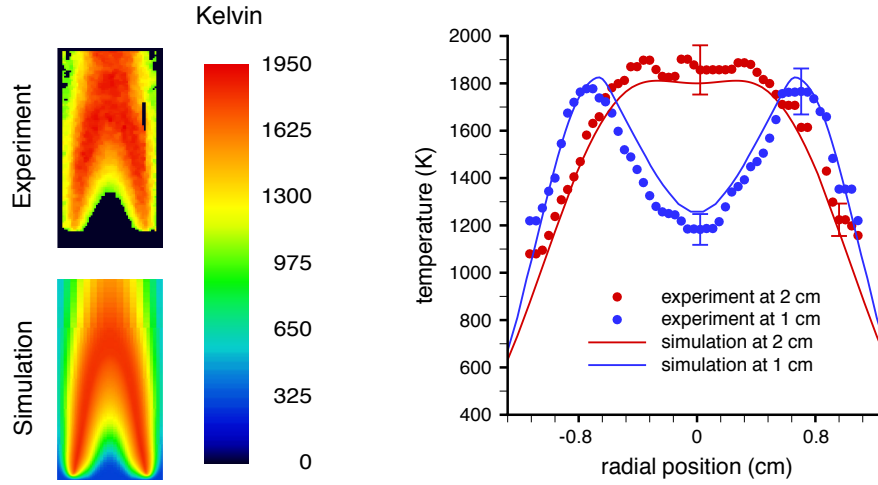


Figure 1: *Experimental and computed temperature fields. (Left) The two-dimensional region shown extends to a radius of 8 mm with a height from 0 mm to 30 mm above the nozzle exit. The experimental field is black where signal/noise was too low for evaluation. (Right) Cross-sections of the experimental and computed temperature fields at two elevations above the nozzle, 1 and 2 cm. Experimental error bars are $\pm 5.5\%$.*

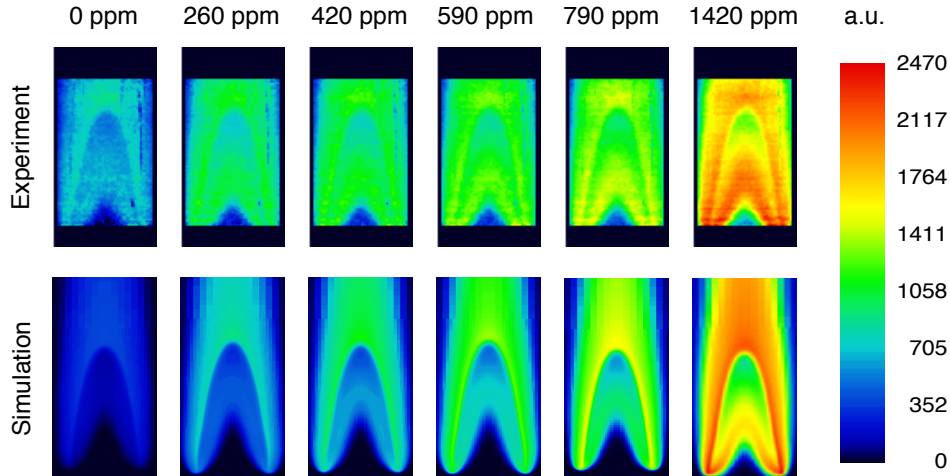


Figure 2: *$\text{NO A-X}(0,0)$ excitation LIF images obtained (top) from measurement and (bottom) by synthetically processing the results of the flame simulation, for different NH_3 seeding concentrations. The experimental data and the synthetic LIF intensities are prepared independently; the same scale applies to both.*

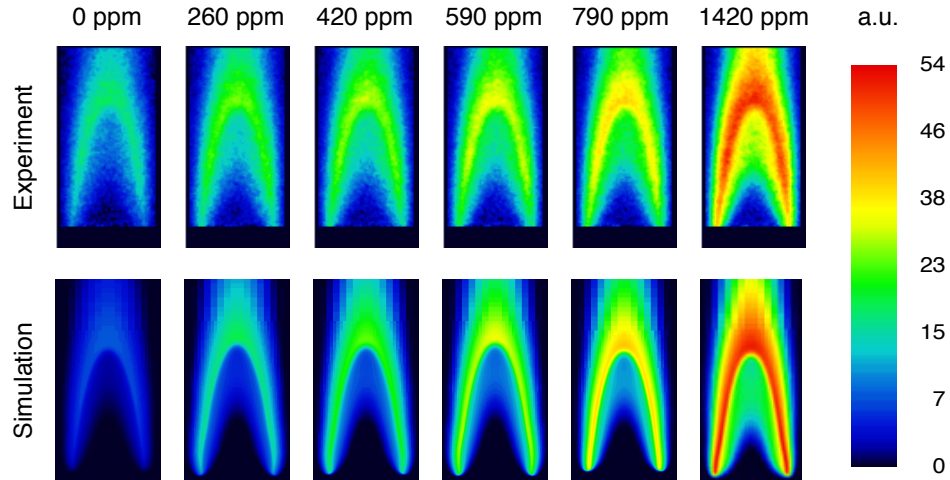


Figure 3: *NO A-X(0,2) excitation LIF images obtained (top) from measurement and (bottom) by synthetically processing the results of the flame simulation, for different NH_3 seeding concentrations. The experimental data and the synthetic LIF intensities are prepared independently; the same scale applies to both.*

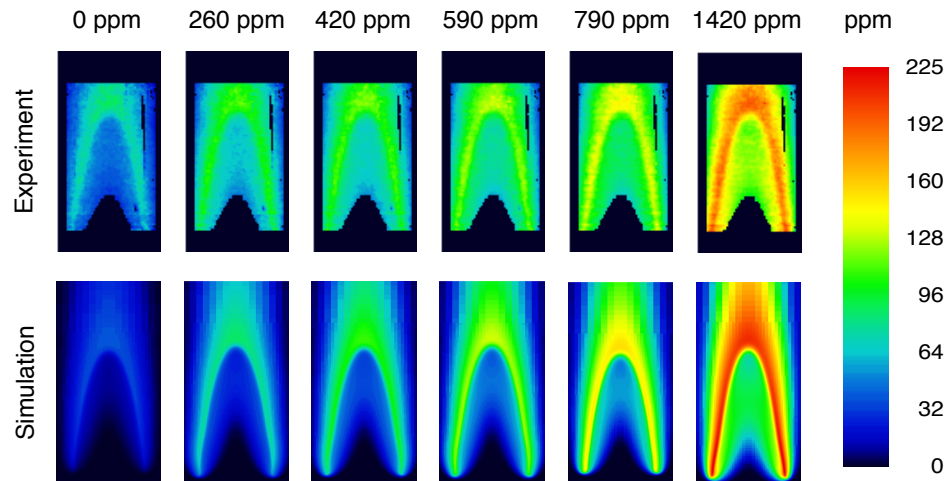


Figure 4: *Experimental and computed NO concentration fields (ppm) for various levels of NH_3 seeding in the fuel stream.*

